Electronic Supplementary Material (ESI) for Journal of Materials Chemistry C.

Straddling $SnSe_2/SnS_2$ van der Waals tunneling heterostructures for high performance broadband photodetectors

Xiangna Cong [a], *Muhammad Najeeb Ullah Shah*[b] *and Wenlong He*[a,*]

[a]*Key Laboratory of Optoelectronic Devices and Systems of Ministry of Education and Guangdong Province, College of Physics & Optoelectronic Engineering, Shenzhen University, Shenzhen 518060, China*

[b]*International Collaborative Laboratory of 2D Materials for Optoelectronics Science and Technology of Ministry of Education, Institute of Microscale Optoelectronics, Shenzhen University, Shenzhen 518060, China*

[*]Authors to whom correspondence should be addressed.

Electronic mail: wenlong.he@szu.edu.cn

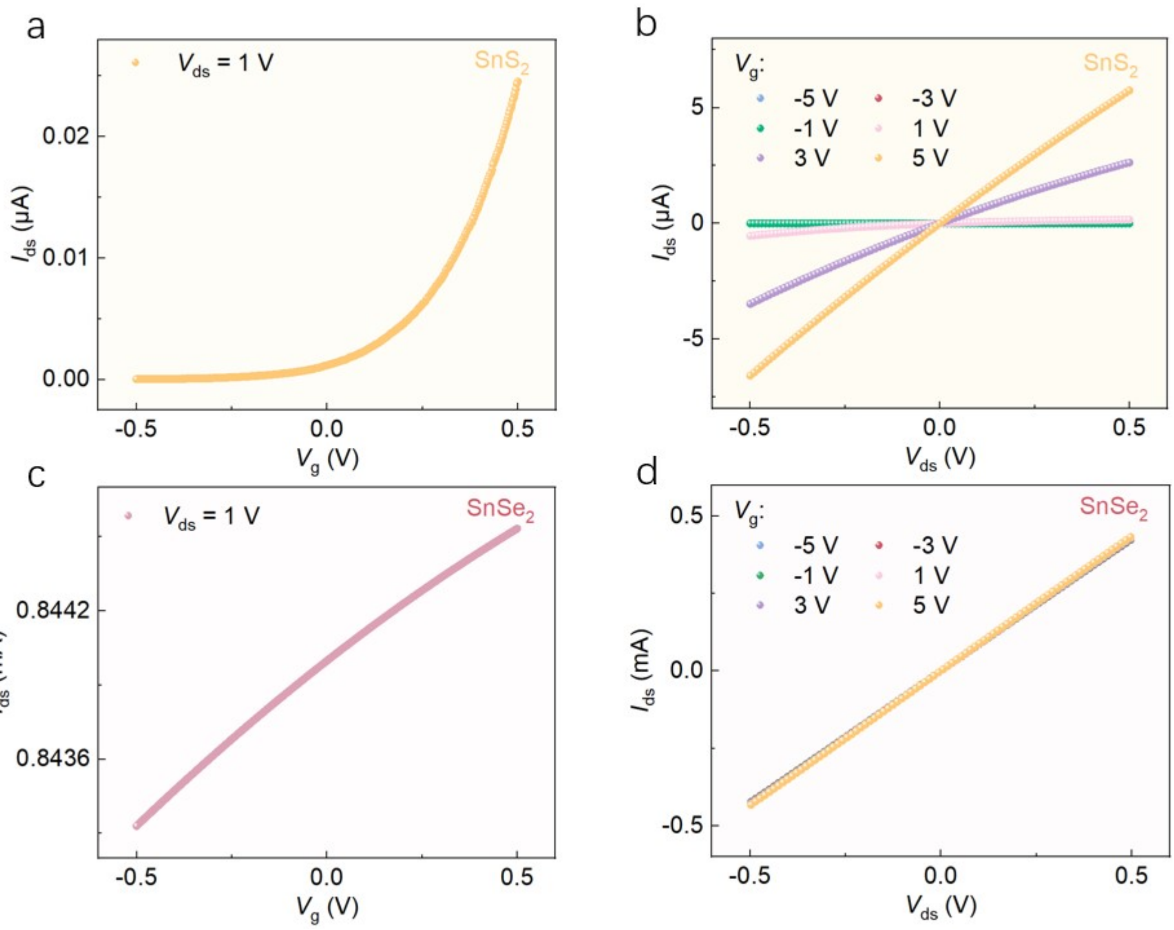

Figure S1 The transport and output curves of SnS_2 (a, b) and $SnSe_2$ (c, d) for $SnSe_2$/SnS_2/h-BN/graphene heterostructure.

In order to enhance the comprehension of the charge transfer mechanism in the SnS_2 and $SnSe_2$ heterostructure, electrical measurements are applied on individual SnS_2 and $SnSe_2$ flakes. The output and transfer curves of SnS_2 and $SnSe_2$ are shown in Figure S1. It is observed that the gate voltage has a significant impact on the SnS_2 current, implying that the Fermi level of SnS_2 can be readily modulated by the gate voltage. The $SnSe_2$ transfer curve exhibits n-type conduction characteristics, with a high drain current and minimal modulation within the gate voltage range of -5 to 5 V (Figure S1c), implying that a high electron density and a Fermi level situated close to the $SnSe_2$ conduction band minimum.

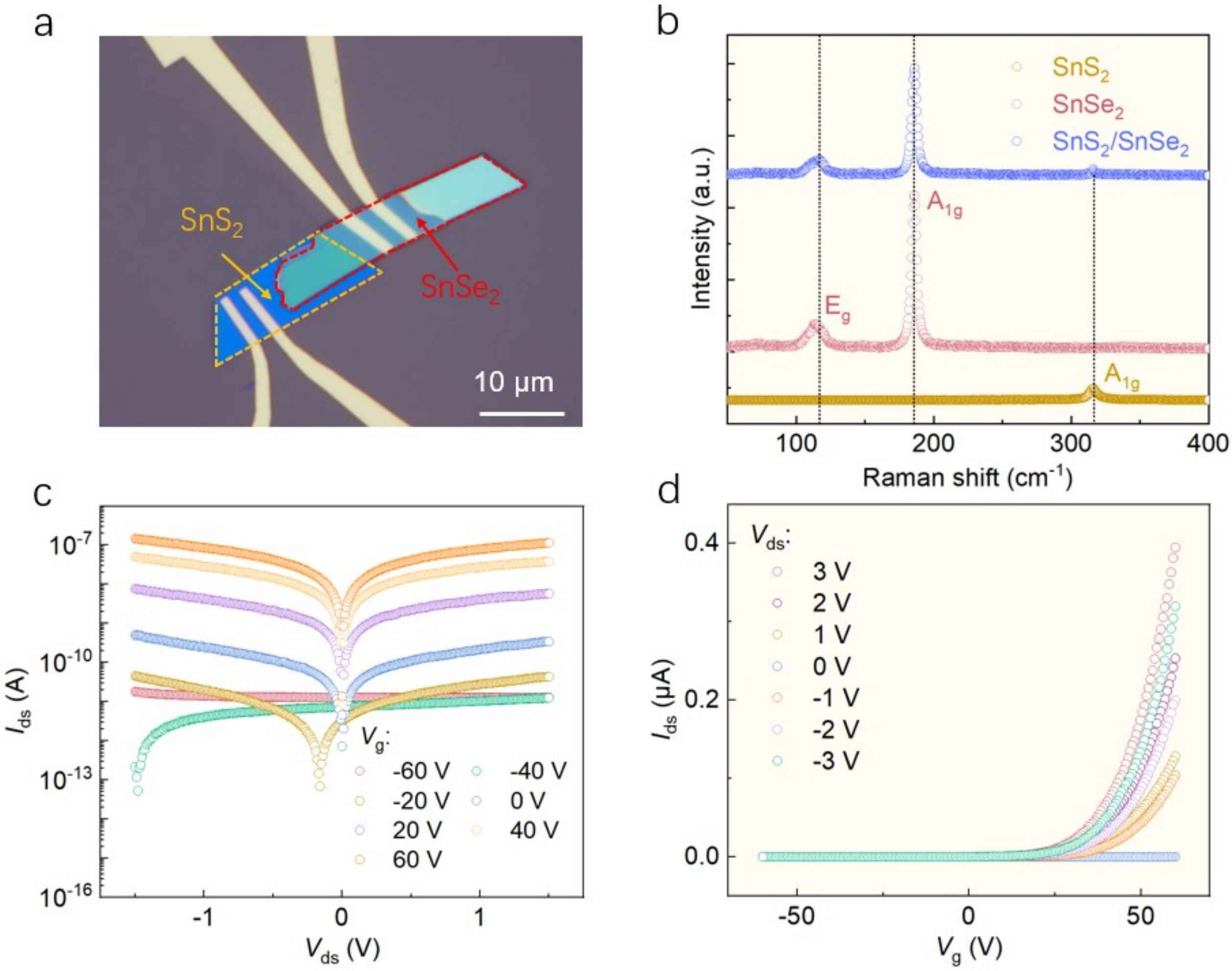

Figure S2 (a) Optical image of the $SnSe_2/SnS_2$ heterostructure. (b) Raman spectra of the $SnSe_2/SnS_2$ heterostructure. The output (c) and transport (d) curves for $SnSe_2/SnS_2$ heterostructure.

Figure S2c-S2d illustrates the electrical characteristics of the $SnSe_2/SnS_2$ heterostructure at various voltages. The currents exhibit a decreasing trend as the V_g decreases, indicating the gate tunability of the $SnSe_2/SnS_2$ heterostructure in Figure S2c.

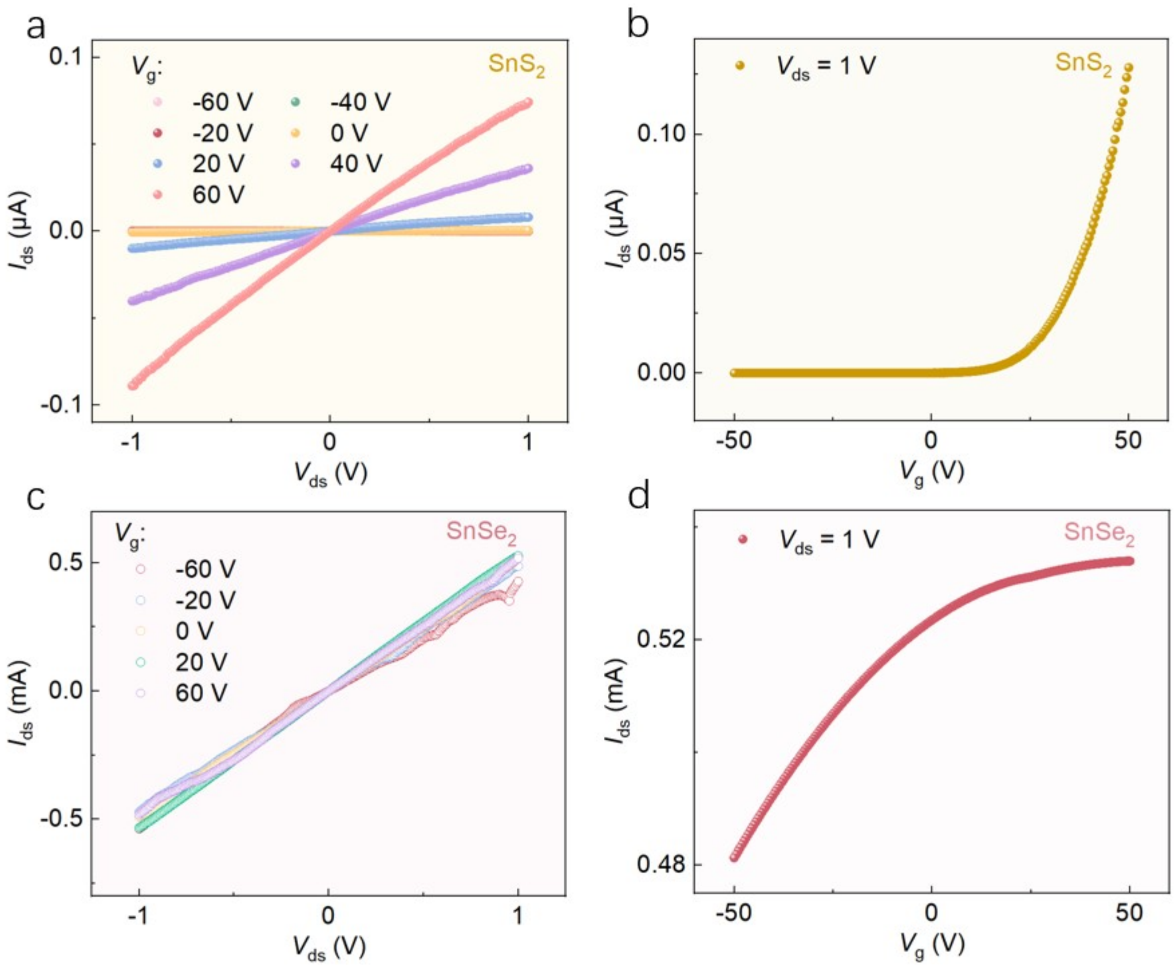

Figure S3 The output and transport curves of SnS_2 (a, b) and $SnSe_2$ (c, d) for $SnSe_2/SnS_2$ heterostructure.

According to Figure S3, the output characteristics of the $SnSe_2/SnS_2$ heterostructure are investigated under varying gate voltage. Notably, the current of SnS_2 demonstrates a substantial variation across different gate voltages, indicating that the current is predominantly modulated by the gate voltage. The transfer characteristics of $SnSe_2$ (SnS_2) under a gate voltage of 1V demonstrate n-type semiconductor behavior. This indicates that the material exhibits characteristics associated with electron conduction.

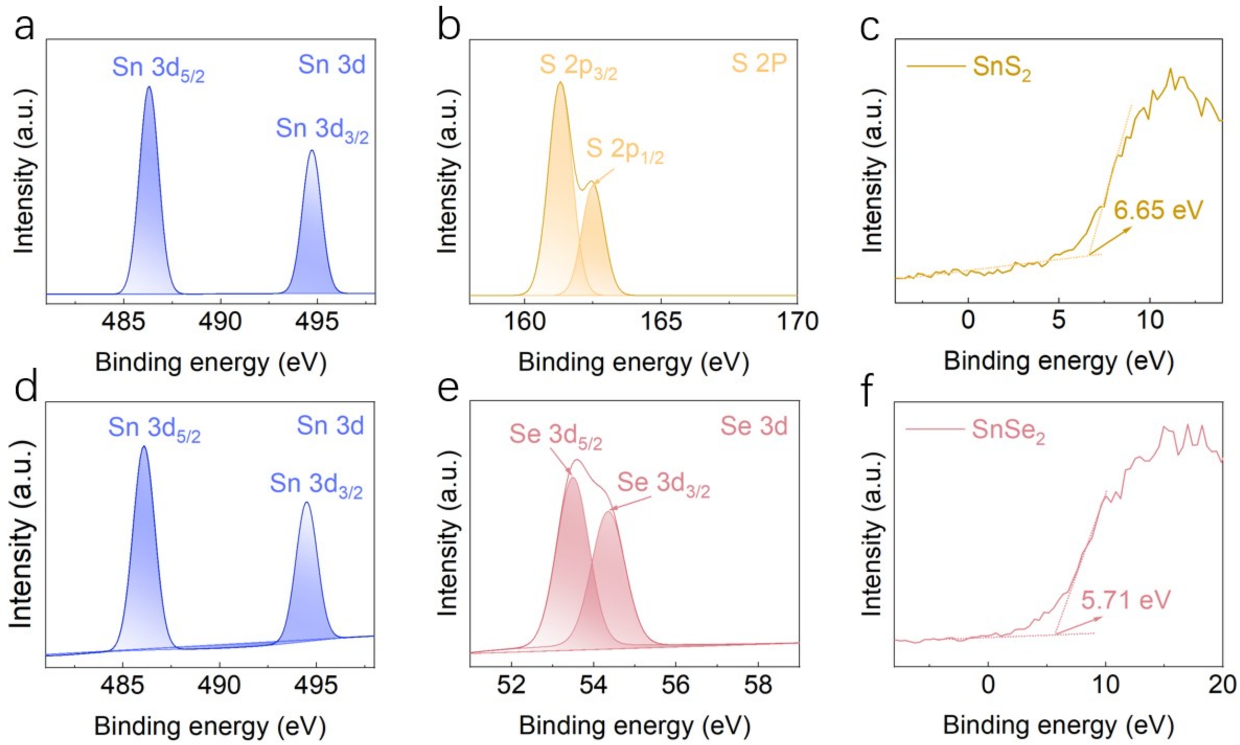

Figure S4 XPS spectra of (a) Sn 3d, (b) S 2p in SnS_2, (d) Sn 3d, (e) Se 3d in $SnSe_2$, valence band spectra of (c) SnS_2, (f) $SnSe_2$.

The X-ray photoelectron spectroscopy (XPS) spectra of SnS_2 and $SnSe_2$, are illustrated in Figure S4. In the SnS_2 heterostructure, the characteristic peaks of the S element are attributed to the S $2p_{3/2}$ (161.31 eV) and S $2p_{1/2}$ (162.52 eV) (Figure S4b), respectively. Additionally, the peaks of Se element at 53.49 eV (Se $3d_{5/2}$) and 54.35 eV (Se $3d_{3/2}$) correspond to $SnSe_2$ (Figure S4e). To validate the band structure, we assess the valence band spectra of both SnS_2 and $SnSe_2$, the valence band maximum values of 6.65 eV and 5.71 eV for SnS_2 (Figure S4c) and $SnSe_2$ (Figure S4f) are conducted.

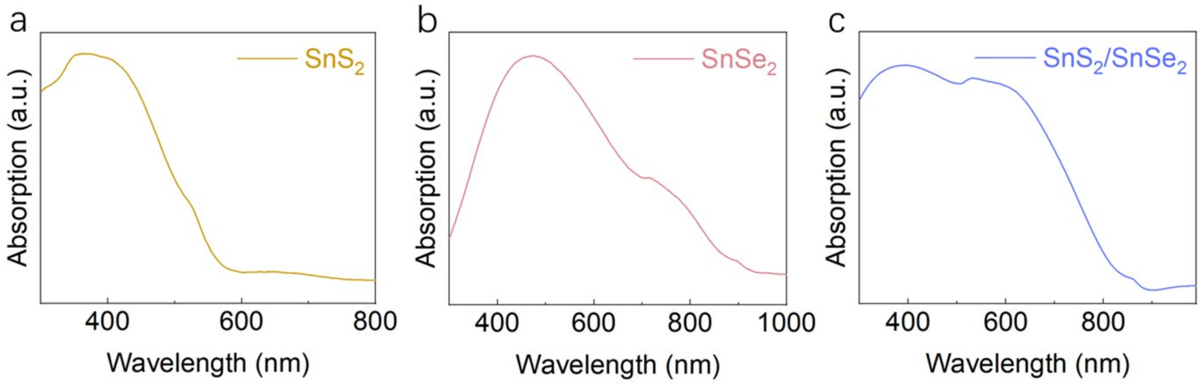

Figure S5 Absorption spectra of (a) SnS_2, (b) $SnSe_2$ and (c) $SnS_2/SnSe_2$ heterostructure.

By analyzing the absorption spectra (as illustrated in Figure S5), SnS_2 exhibits a broad absorption peak spanning from 350 nm to 500 nm, indicating that its remarkable optical absorption characteristics across the ultraviolet-visible spectrum. $SnSe_2$ has the light absorption peak in the range of ultraviolet-visible spectrum, featuring a pronounced absorption peak at wavelengths between 400 nm and 700 nm. A noticeable expansion in the range of light absorption is found in the $SnSe_2/SnS_2$ heterostructure, with heightened absorption intensity particularly in the visible region, which signifies the potential of the $SnSe_2/SnS_2$ heterostructure in the realm of optoelectronic devices.

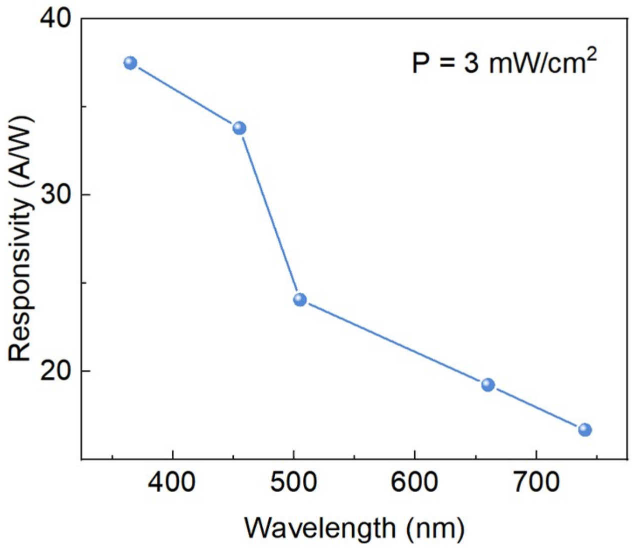

Figure S6 Responsivity as a function of wavelengths for the $SnSe_2/SnS_2$/h-BN/graphene heterostructure.

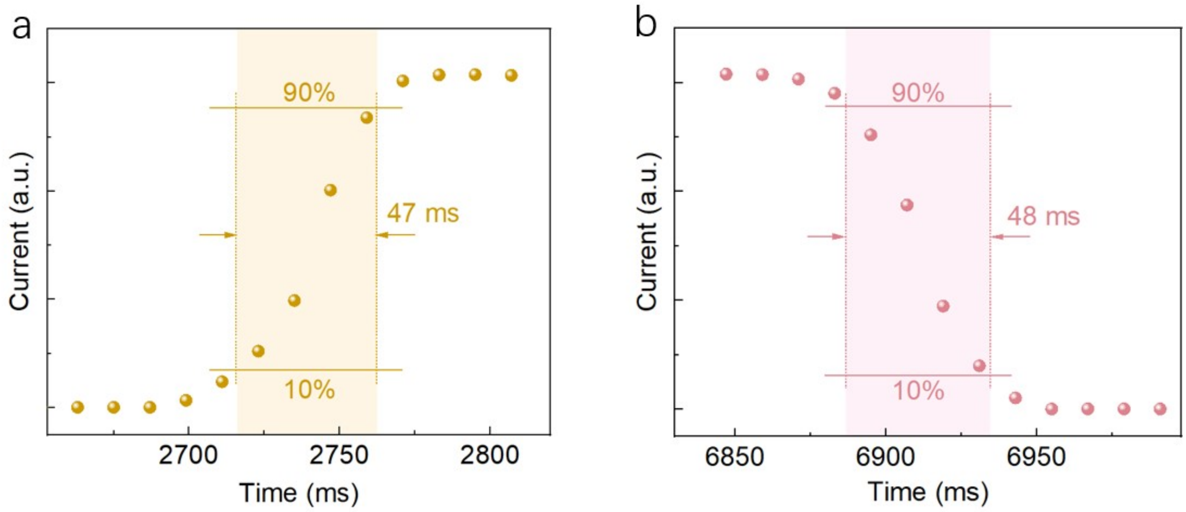

Figure S7 The rise (a) and decay time (b)of the $SnSe_2/SnS_2$ heterostructure.

Table S1 Comparison the parameters of various type I-III vdW heterostructures photodetectors.

Materials	**Type**	**Wavelength (nm)**	**R (A/W)**	**On/off ratio**	**D* (Jones)**	**τ_r (ms)**	**τ_d (ms)**	**Reference**
WS_2/h-BN/$PdSe_2$	-	520	-	10^6	$2.7x10^{12}$	-	-	1
GaTe/InSe	II	1064	267.4	-	10^{14}	10^3	10^3	2
BiI_3/BiI	II	638	1	$>10^3$	$8.8x10^{12}$	0.00382	0.00467	3
SnS_2/MoS_2	II	532	28	10^6	$4x10^{11}$	640	410	4
$MoTe_2/SnSe_2$	III	885	36	10^5	$1.03x10^{12}$	10	12	5
$PdSe_2/MoS_2$	II	532	9	-	$3x10^{10}$	125	7	6
WS_2/PtS_2	I	653	0.33	$>10^5$	$4.3x10^{10}$	55	54	7
GeSe/MoS_2	II	532	0.105	10^4	$1.46x10^{10}$	110	750	8
InSe/ReS_2	-	365	1921	-	$6.51x10^{13}$	21.6	43.2	9
WSe_2/MoS_2	II	532	2700	10^2	$5x10^{11}$	17	29	10
InSe/$PdSe_2$	II	1650	58.8	-	$1x10^{10}$	160	180	11
WSe_2/ReS_2	II	532	3	-	$8.39x10^{10}$	0.005	0.005	12
$SnSe_2/SnS_2$	I	365	37.5	10^7	$1.2x10^{10}$	47	48	This work

References

1 Y. Chen, Y. Wang, Z. Wang, Y. Gu, Y. Ye, X. Chai, J. Ye, Y. Chen, R. Xie, Y. Zhou, Z. Hu, Q. Li, L. Zhang, F. Wang, P. Wang, J. Miao, J. Wang, X. Chen, W. Lu, P. Zhou and W. Hu, *Nat Electron*, 2021, **4**, 357–363.

2 T. Qi, Y. Gong, A. Li, X. Ma, P. Wang, R. Huang, C. Liu, R. Sakidja, J. Z. Wu, R. Chen and L. Zhang, *Adv Funct Materials*, 2020, **30**, 1905687.

3 H. Mu, R. Zhuang, N. Cui, S. Cai, W. Yu, J. Yuan, J. Zhang, H. Liu, L. Mei, X. He, Z. Mei, G. Zhang, Q. Bao and S. Lin, *ACS Nano*, 2023, **17**, 21317–21327.

4 S. Quan, L. Li, S. Guo, X. Zhao, D. Weller, X. Wang, S. Fu, R. Liu and Y. Hao, *ACS Appl. Mater. Interfaces*, 2023, **15**, 59592–59599.

5 X. Cong, Y. Zheng, F. Huang, Q. You, J. Tang, F. Fang, K. Jiang, C. Han and Y. Shi, *Nano Res.*, 2022, **15**, 8442–8450.

6 H. Wang, Z. Li, D. Li, X. Xu, P. Chen, L. Pi, X. Zhou and T. Zhai, *Adv Funct Materials*, 2021, **31**, 2106105.

7 Z. Wang, H. Zhang, W. Wang, C. Tan, J. Chen, S. Yin, H. Zhang, A. Zhu, G. Li, Y. Du, S. Wang, F. Liu and L. Li, *ACS Appl. Mater. Interfaces*, 2022, **14**, 37926–37936.

8 Y. Xin, X. Wang, Z. Chen, D. Weller, Y. Wang, L. Shi, X. Ma, C. Ding, W. Li, S. Guo and R. Liu, *ACS Appl. Mater. Interfaces*, 2020, **12**, 15406–15413.

9 H. Ma, Y. Xing, J. Han, B. Cui, T. Lei, H. Tu, B. Guan, Z. Zeng, B. Zhang and W. Lv, *Advanced Optical Materials*, 2022, **10**, 2101772.

10 G. H. Shin, C. Park, K. J. Lee, H. J. Jin and S.-Y. Choi, *Nano Lett.*, 2020, **20**, 5741–5748.

11 W. Ahmad, J. Liu, J. Jiang, Q. Hao, D. Wu, Y. Ke, H. Gan, V. Laxmi, Z. Ouyang, F. Ouyang, Z. Wang, F. Liu, D. Qi and W. Zhang, *Adv Funct Materials*, 2021, **31**, 2104143.

12 A. Varghese, D. Saha, K. Thakar, V. Jindal, S. Ghosh, N. V. Medhekar, S. Ghosh and S. Lodha, *Nano Lett.*, 2020, **20**, 1707–1717.